The Influence of Iron Concentration on the Anodic Charge Transfer in Molten Oxide Electrolysis

Jan Wiencke, Hervé Lavelaine, Pierre-Jean Panteix, Carine Petitjean, Christophe Rapin

The Influence of Iron Concentration on the Anodic Charge Transfer in Molten Oxide Electrolysis

Jan Wiencke*[1,2], Hervé Lavelaine[1], Pierre-Jean Panteix[2], Carine Petitjean[2], Christophe Rapin[2]

** Corresponding author, Email-address: Jan.wiencke@arcelormittal.com*
[1]Dept. of Ironmaking, Global Research and Development ArcelorMittal, Maizières-lès-Metz, France (FR)
[2] Université de Lorraine, IJL-UMR 7198, Département CP2S, 54000 Nancy, France

Abstract

The anodic charge transfer during the production of iron by Molten Oxide Electrolysis in an Al_2O_3-MgO-SiO_2 electrolyte has been investigated at 1793 K in dependence of the iron oxide concentration. Experiments were performed at laboratory scale using an asymmetric electrode configuration. The kinetic relation to the cell voltage was analyzed by a stepped linear scan voltammetry at various iron oxide concentrations up to 15 wt%. Complementary gas analysis allowed the derivation of the oxygen production yield.

The obtained results show an electronic contribution to the overall conduction. This contribution diminishes in proportion with increasing iron oxide concentration. Charge transfer at the anode is accomplished by the oxidation of ferrous iron ions and of oxide anions. Conditions for the electrochemical charge transfer to occur solely by the oxidation of oxide anions exist for a limited cell voltage range at iron oxide concentrations of less than 10 wt%. For these concentrations a mass transfer limitation of oxide anions was detected with increasing cell voltage. However, a limit of the total current is absent as

ferrous iron participates to the anode charge transfer at cell voltages above the mass transfer limitation of oxide ions.

Introduction

Molten oxide electrolysis (MOE) is a possible way to extract metal from its ore using electricity [1-4]. Numerous studies have demonstrated its potential for the reduction of CO_2 emission in industrial processes, e.g. in the steel industry [5-6]. The feed oxide is dissolved in the molten oxide electrolyte and its decomposition into oxygen and metal occurs via

$$M_xO_y \leftrightarrows xM + {}^{y}/_{2}O_2 \qquad (1)$$

Assuming the oxides are disassociated in the melt, the electrode half reactions would then follow

$$\text{Cathode:} \quad M^{(II)} + 2e^- \rightarrow M \qquad (2)$$

$$\text{Anode:} \quad 2O^{(II-)} \rightarrow O_2 + 4e^- \qquad (3)$$

While the electrochemical signature of reaction (2) depends on the metal produced, reaction (3) is of more general importance to the process. Evidence has shown that the anode half reaction in MOE is controlled by the diffusion of free oxide anions (O^{II-}) in the melt towards the electrode [7], which infers a strong dependence on the electrolyte's optical basicity [8-9]. However, the oxygen production itself was not monitored during these experiments and either the conditions (i.e. PO_2, reactive cell constituents) did not allow multivalence of any of the present components or their concentration was kept too low for them to interfere with the anode half reaction. Extraction of transition metals, such

as Fe or Mn, will be executed at a higher concentration of the feed oxide. Thus, the corresponding ion, then present in multivalence, is likely to participate in the anode half reaction [10]. Continuous oxidation of the target metal cation would be critical for metal production as it invokes electronic conduction in the electrolyte [11], causing thereby a loss of the process faradaic yield.

The present work focusses on the anodic behavior of molten oxides with increasing contents of a transition metal, namely iron. For this purpose, a composition of the ternary system Al_2O_3-MgO-SiO_2, proven suitable for metal production [12], was chosen and investigated by stepped linear scan voltammetry with an asymmetric electrode configuration. The electrochemical measurements were accompanied by a life measure of the oxygen production. This allows the quantification of the faradaic yield, which gives a direct insight on the impact of iron concentration on the anode half reaction.

Materials and Methods

The experimental plan

To determine the anode half reaction during iron metal production by MOE an experimental series was carried out with a geometrically asymmetric electrode setup. Motivation to use this type of setup was given by the ability to characterize the reaction at the working electrode without the requirement for a reference electrode [13], which is not existent in iron-bearing molten oxides [7]. A large surface cathode was therefore used in this study and the different electrolytes were characterized by Stepped Linear Scan Voltammetry (SLSV). The acquired electrochemical signal was accompanied by a

measurement of the oxygen gas production. By the combination of the electrochemical and the oxygen signal it is then possible to fully describe the anode half reaction of the MOE process. A more comprehensive description of this experimental methodology is given in a preceeding study [14], where the same approach had been applied to determine the kinetics of the cathodic reduction of ferrous iron into liquid metal iron at 1823 K.

Preparation of the electrolyte

The electrolyte was prepared from oxide powders, their chemical sources are listed in Table 1. An iron-free composition (Fe#0) was used as starting material. To ensure homogeneity, this composition was prepared by two pre-melting procedures at 1873 K with a subsequent rapid quench at air on a steel plate. The glass was milled into powder after each fusion with a planetary ball mill (the containing vessel made of agate). To this powder mixture, varying amounts of iron oxide were added. The compositions of Fe#0, the different electrolytes and their respective optical basicity (Λ) are given in Table 2. The optical basicity of the different electrolytes was calculated using the data of Duffy and Ingram [15].

The electrochemical cell

The electrochemical cell consisted of an alumina crucible, 28 mm in diameter, with a round bottom through which the cathode electrical lead, a Pt30Rh wire with a 1 mm diameter, was inserted. At the bottom of the alumina crucible a solid piece of iron was placed, serving as the cathode for the experiment. This piece of iron metal was prepared by a pre-melting step in which 41 gr of iron flakes (purity 99.98%) were melted at 1873 K in the crucible under an argon atmosphere. The resulting geometry then matched the form of

the crucible with an electrode surface facing the anode with 530 mm^2. The anode, a Pt10Rh rod with a 3 mm diameter, was immersed 5 mm into the electrolyte from atop leading to an electrode surface of 54 mm^2 in contact with the electrolyte. Argumentation for the choice of the materials is given by their thermal and chemical stability at experimental conditions. For further detail, the reader is referred to a previously published study [12].

The anode was inserted into the melt at the operating temperature and its immersion depth was determined by the establishment of electrical contact. This was achieved by monitoring the open circuit potential, which revealed the moment of contact between the electrode and the electrolyte's surface by a sharp shift in the signal's behavior. Displacement of the anode using a micrometer then allowed its exact positioning. A schematic drawing of the electrochemical cell is presented in Figure 1.

To illustrate the electric field within the cell, the equi-potential-lines ($V_{Equi.}$) and Constant Streamline Functions ($CSF_{Equi.}$) were determined using the software ELDEP© and subsequent Finite Element calculations, Figure 2. The geometrical factor K for this cell, determined by means of Laplace equation, is equal to 0.62 S cm^{-1}. The majority of the ohmic drop occurs at the anode, rendering the cathode's overpotential negligible in comparison. The electrochemical response acquired in this cell can thus be understood as the result of the ohmic drop in the electrolyte and the overpotential at the anode. A more detailed explanation of the derivation of the different parameters is given in a previous study [14].

Experimental assemblage and used analysis techniques

Experiments were conducted in a vertical tube furnace, which was flushed with an Argon gas flow (Westfalen, Ar: 99.998% O_2:3 ppm). A gas flow-rate was maintained at 0.05 $m^3.h^{-1}$, given standard conditions (STP), defined for atmospheric pressure and temperature of 273.15 K. Experiments were performed in the isothermal region of the tube furnace (~8 cm along z-axis of the furnace) and the temperature was measured via a B-type thermocouple. The concentration of O_2 gas in the furnace chamber was measured by an oxygen analyzer that was connected to the gas circuit downstream to the furnace. Schematic drawings and further specifications of the experimental aperture are given elsewhere [12, 14].

The desired electrochemical conditions in the experimental cell were applied using a potentiostat (model VersaStat 3, Ametek). The cell voltage interval for the SLSV is defined as 0.8-1.9 V. For each step in the SLSV, the cell voltage was increased by 20 mV. The step-length was 600 s (effective scanning rate 0.03 $mV.s^{-1}$). Values of each cell voltage used for calculation were obtained by taking the average of the second half of each cell voltage increment, at which point current values had generally stabilized. Reasoning for the use of such long increments is given by the travel time of evolved oxygen gas from the anode to the O_2-analyzer. This transport time can be several minutes depending of the electrolyte composition and its viscosity. Two identical experiments were performed for each electrolyte composition to evaluate the reproducibility of the results.

Results

Figure 3 displays the measured current density acquired during the SLSVs. Results show a good reproducibility for the different compositions. With increasing iron oxide content, the current density increases. It is observed that compositions Fe#5 and Fe#7.5 behave similarly in dependence of the applied cell voltage. Current density starts to increase at about 1.1 V with a monotonic; however, continuously, diminishing slope. Fe#15 differs from this trend by exhibiting three distinct sections in the cell voltage ranges 0.8-1.0 V, 1.0-1.2 V and 1.2-1.9 V. While the first and third section exhibit a similar slope, the second is characterized by a steeper increase of current density. Fe#10 conducts as an intermediate between these two cases, showing a steep increase between 1.05-1.15 V and thereafter a monotonic increase with decreasing slope.

The measured current density below 1 V is presented in the inset of

Figure 3. A nearly linear dependence of the current density on the cell voltage can be observed in all compositions. While the magnitude increases proportionally with iron content in the compositions Fe#5, Fe#7.5 and Fe#10, acquired values for Fe#15 are significantly elevated.

The concentration of oxygen measured within the argon gas flow during the SLSVs are shown in

Figure 4. Its magnitude is linked to the iron oxide content of the electrolyte. All experiments can be divided into two main segments. The first ends at approximately 1 V and is described by a continuous decrease in O_2 concentration. The measured concentration can be attributed to the process of thermal decomposition of the magnetite during heating [12, 16] following

$$2Fe_3O_4 \leftrightarrows 6FeO + O_2 \qquad (4)$$

This process started during the heating of the sample and once the operating temperature was reached most of the oxide had already been thermally decomposed into FeO and the impact of the reaction diminished. Therefore, O_2 levels decreased with ongoing experimental duration. The second segment is characterized by an increase of O_2 levels augmented by the cell voltage.

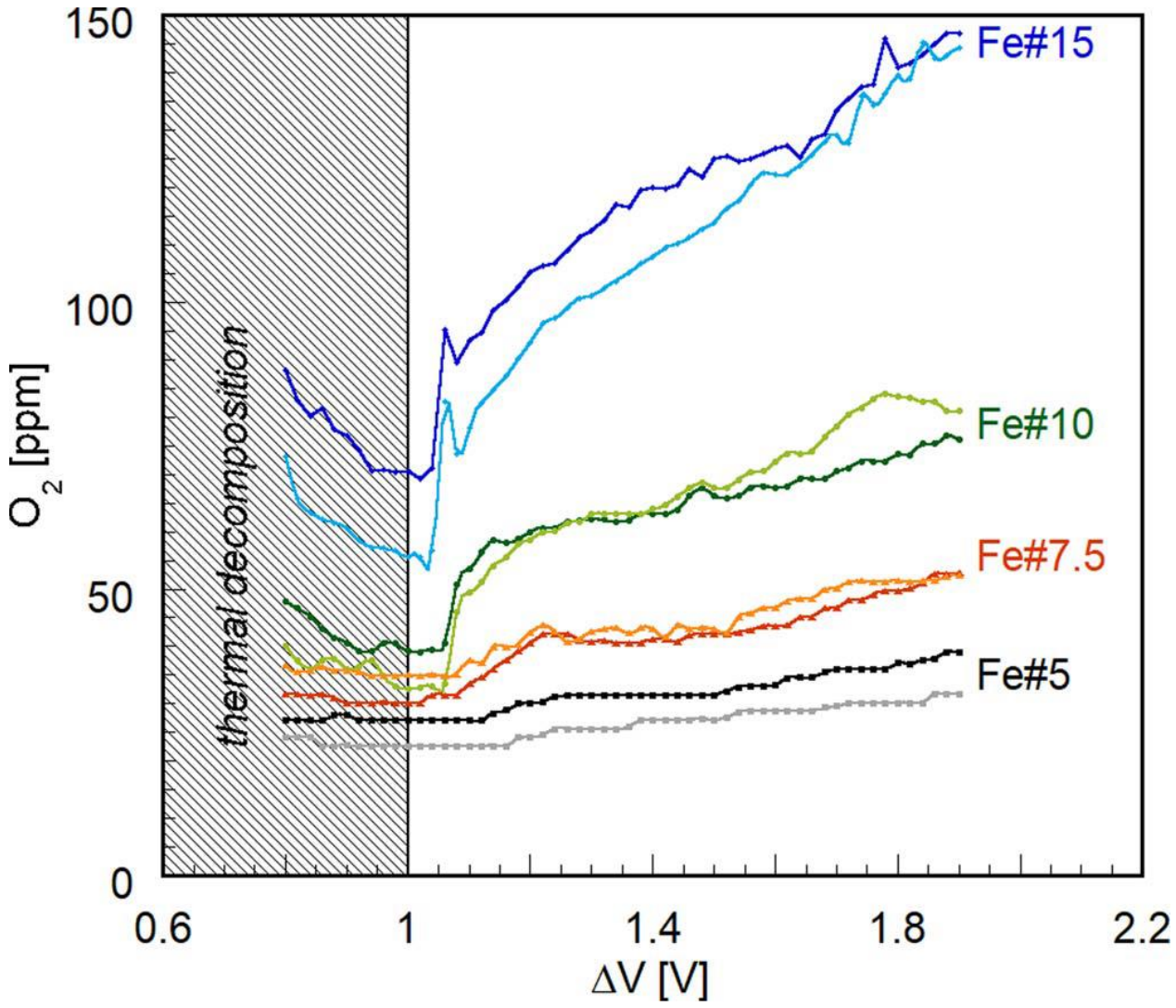
150
100
50
0
O2 [ppm]
thermal decomposition
Fe#15
Fe#10
Fe#7.5
Fe#5
0.6
1
1.4
1.8
2.2
ΔV [V]

Figure 5 is a micrograph of the cooled down electrochemical cell after the experiment with Fe#15. The iron metal cathode is below the partially crystallized electrolyte. Light zones in the electrolyte mark either fractures of the solidified oxide or zones of pronounced crystallization. It can be observed that the electrolyte stayed entirely on top of the cathode and did not enrobe the metal piece. Furthermore, the corrosion of the alumina refractory is limited. The missing part of the left crucible wall had to be cut off with a saw during sample preparation.

Discussion

Description of the anode half reaction

During the SLSV a significant amount of the electric charges have been transferred through the different molten oxide electrolytes. Charge transfer in molten oxides can occur as electronic conduction (i.e. electron hopping) and ionic conduction (i.e. the diffusion of ions) [11, 17]. Electron hopping is a non-faradaic charge transfer and leads to a loss of the MOE process yield. The compositions investigated here were chosen due to their low electronic contribution [14, 18], to maintain the performance of MOE with a high faradaic yield. The ionic charge transfer is imperatively linked to the electrochemical reactions at the electrodes and occurs solely if the thermodynamic threshold of the cell reaction, ΔE, is exceeded. Determination of ΔE is done via

$$\Delta E = \frac{\Delta G^0}{nF} + \frac{RT}{nF} ln\left[\Pi_i a_i^{\nu i}\right] \qquad (5)$$

where ΔG^0 is the Gibbs energy of the considered reaction in a pure component state [J mol^{-1}], F the Faraday constant [C mol^{-1}], $\Pi_i a_i^{\nu i}$ the product of the activities with ν_i the

stoichiometric coefficient of compound “i”, n the number of electrons involved in the reaction, T the temperature [K] and R the universal gas constant [J mol^{-1} K^{-1}] [19]. At cell voltages below ΔE, negligible charge transfer is expected due to the low electronic conduction in the investigated compositions. Possible electrochemical reactions to occur in the different electrolytes are given in Table 3 together with their thermodynamic potential for each electrolyte. The thermodynamic data for pure compounds was taken from Barin [20] and activities of the different ions in the electrolytes were calculated using the thermochemical software CEQCSI [21].

The cell voltage at the onset of the charge transfer in compositions Fe#5, Fe#7.5 and Fe#10 correlates well with the potential of reaction (8), confer

Figure 3. The anode half reaction would then be the oxidation of oxide anions and the follow reaction (3). The production of oxygen, as seen in

Figure 4, is a confirmation of this reaction occurring.

The current density in Fe#5, Fe#7.5 and Fe#10 acquired above 1 V is characterized by a slope that flattens out towards higher cell voltages,

Figure 3. Despite not reaching a distinct plateau, this trend can be interpreted as a mass transfer limitation of the free oxide anions, which is in coherence with results published elsewhere [7, 9] for lime based molten oxides. In contrast, charge transfer in Fe#15 increases almost linearly and starts significantly below 1 V. Either reaction (6) or reaction (7) are possible to explain the charge transfer in this cell voltage range. The charge transfer at the anode for both reactions would then be accomplished via

$$Fe^{(II)} \rightarrow Fe^{(III)} + 1e^{-} \qquad (13)$$

Additionally at 1 V, reaction (8) occurred, which led to the steep increase in current density observed from 1.0 to 1.2 V. Again, O_2 production, as seen in

Figure 4, can be used as a confirmation for the occurrence of reaction (8).

To quantify the faradaically produced O_2, the measured O_2 concentration had to be corrected for the background O_2. This is done analogue to our previous study [12] where the background level of O_2 was determined by an exponential interpolation between O_2 measured in the cell voltage range 0.8-0.9 V and O_2 measured 1 h after the SLSV. The obtained values were then subtracted from the measured O_2 concentration to obtain $O_{2\,BC}$.

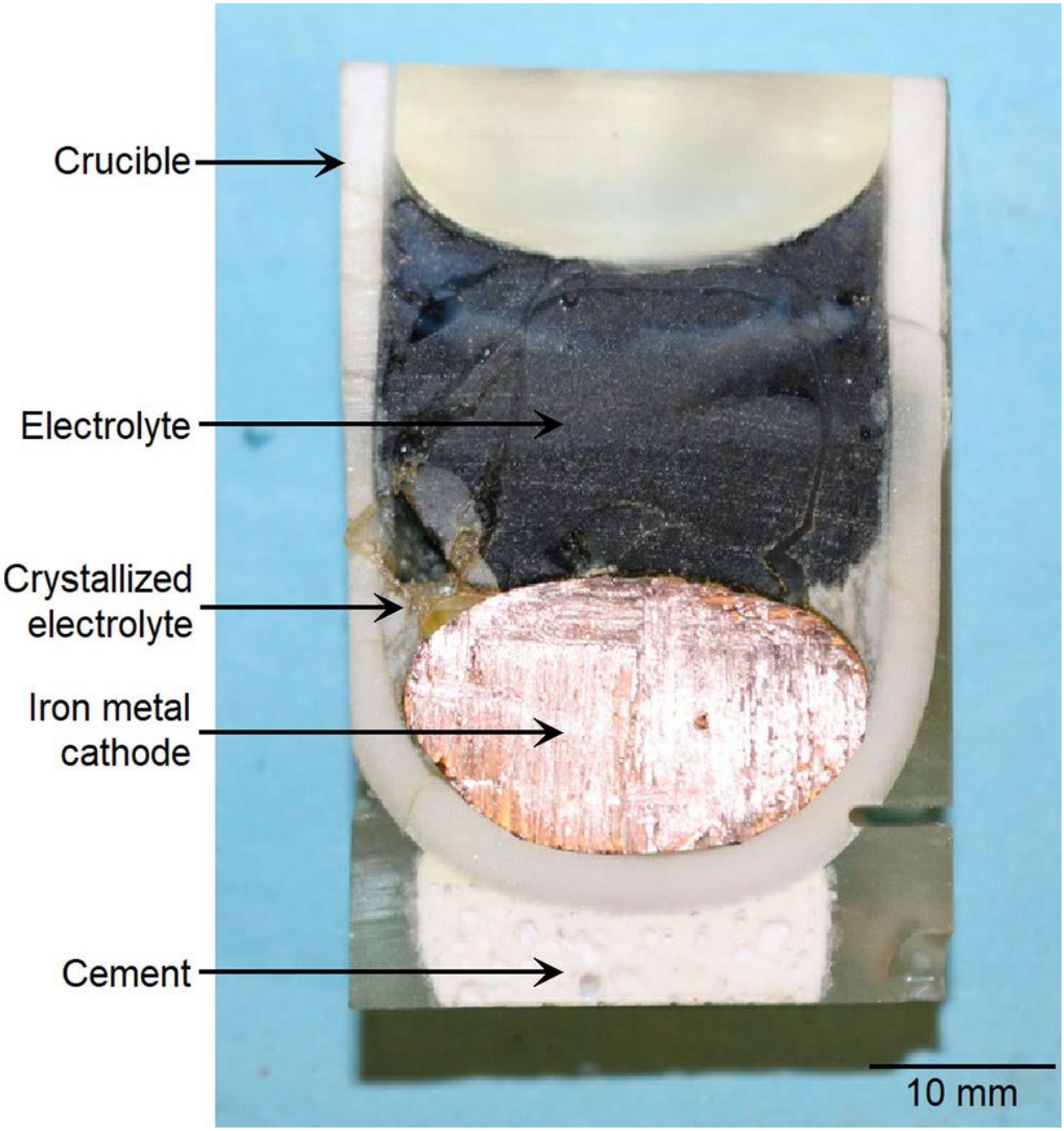
Crucible
Electrolyte
Crystallized electrolyte
Iron metal cathode
Cement
10 mm

Figure **6** shows the background corrected oxygen signal $O_{2\,BC}$. Compositions Fe#10 and Fe#15 exhibit a steep increase of 20 ppm at 1.1 V. Thereafter, both compositions are monotonically increasing. The corrected O_2 signal for Fe#5 and Fe#7.5 were characterized by a shallow increase at 1.1 V until 1.2 V, followed by a subsequent plateau, which extends until 1.5 V. For the remaining interval of the SLSV O_2 increased again. The plateau seen in

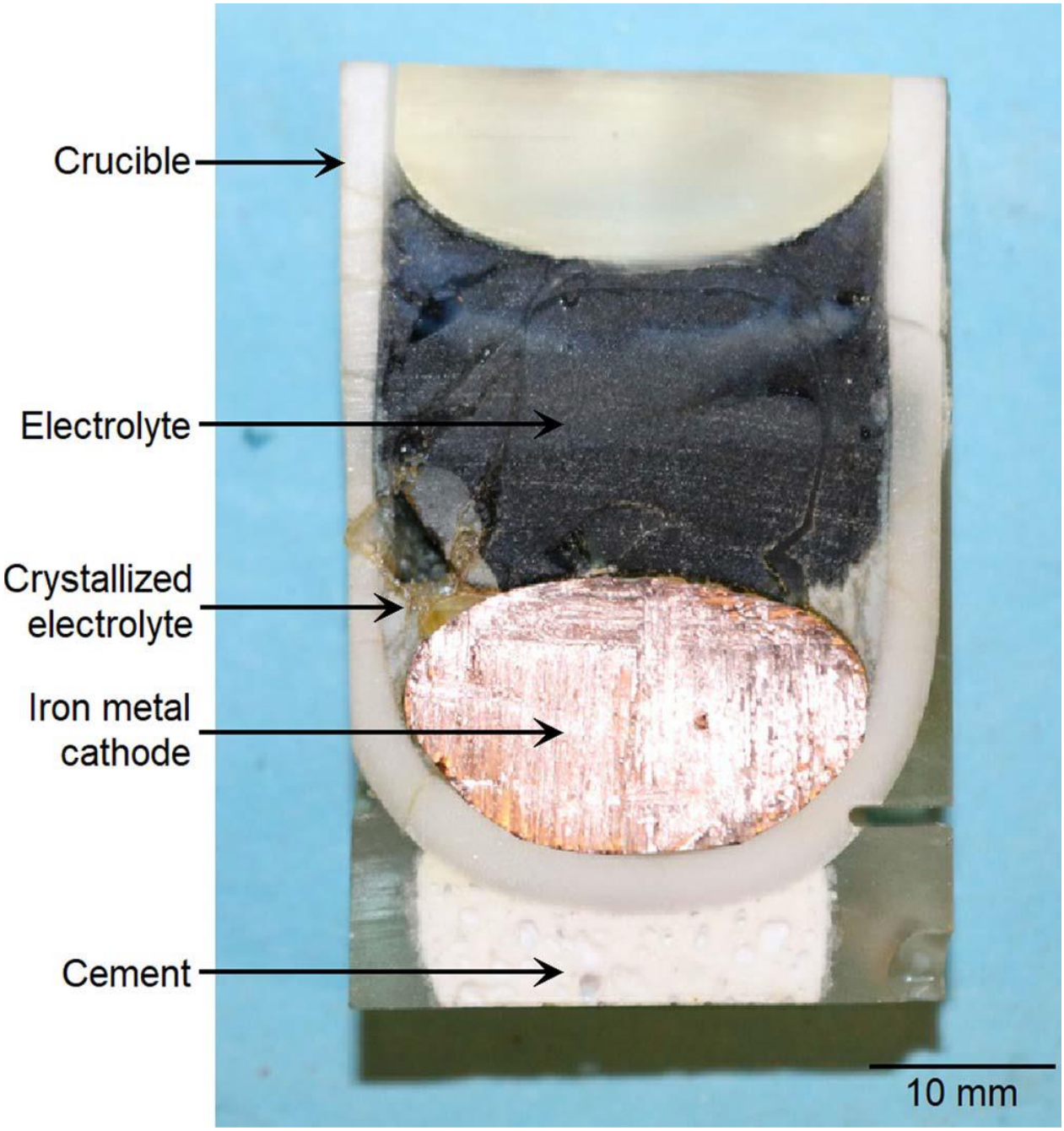
Crucible
Electrolyte
Crystallized electrolyte
Iron metal cathode
Cement
10 mm

Figure **6** for compositions Fe#5 and Fe#7.5 confirms the mass transfer limitation for oxide anions suggested above based on the current density measurement. Its absence in compositions Fe#10 and Fe#15 might indicate an increasing impact of convection close to the anode surface, due to the evolution of O_2 gas. The fact that the O_2 concentration increases again at a cell voltage above 1.5 V in compositions Fe#5 and Fe#7.5 will be discussed separately in the last paragraph.

The faradaic yield for oxygen production

The ratio of the two anode half-reactions, oxidation of oxygen anions via reaction (3) and the oxidation of ferrous iron via (13), expresses the process faradaic yield of O_2 gas production. This faradaic yield, $\#O_2$, is the ratio of the mol[O_2].s^{-1} derived from the background corrected oxygen signal, Q_m, over the mol[O_2].s^{-1} produced by the measured current, Q_{ideal}.

$$\#O_2 = {}^{Q_m}/_{Q_{ideal}} \qquad (14)$$

The yield of O_2 production is displayed in

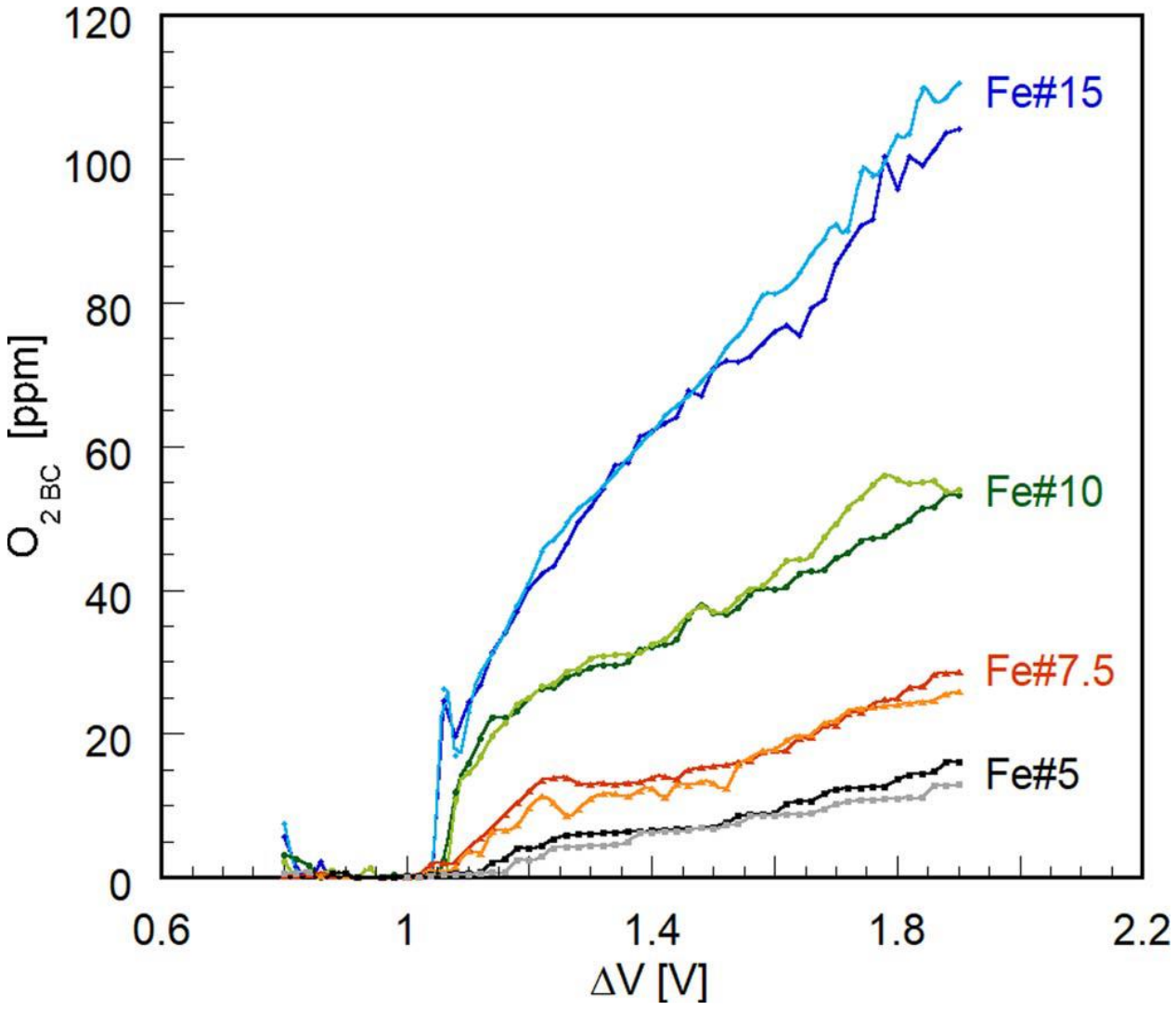

Figure **7** for one of the two SLSV of each electrolyte composition.

In compositions Fe#5, Fe#7.5 and Fe#10 a broad peak is observed in the cell voltage interval 1-1.5 V. The magnitude of this peak increases with iron oxide content. Thereafter, the faradaic yield decreases markedly up to the cell voltage 1.6 V. The faradaic yield of Fe#15 differs in its behavior and is, once O_2 gas is produced, stable throughout the SLSV at a value of ~50%. Generally, it is observed that with increasing iron oxide content the anode yield increases. This result is contra-intuitive as it was expected that with increasing iron content ferrous iron would become more important for the anode half-reaction. The derived result becomes even more suspect, considering that below 1 V all current at the anode is transferred via the oxidation of ferrous iron in Fe#15. Furthermore, there seems to be a discontinuity in the behavior between the composition Fe#10 and Fe#15, indicating a shift in behavior of ferrous iron between those two compositions.

To understand the faradaic yield better, it is necessary to separate the different types of conduction in the cell and mechanisms of charge transfer at the anode. As mentioned in the introduction, electronic and ionic conduction can both take place in the electrolytes. Electronic conduction is not linked to the production of oxygen gas and thus lowers the faradaic yield. Q_{ideal}, which represents the mol[O_2].s^{-1} based on the sum of electronic and ionic current in the electrolyte, has therefore to be corrected for the electronic current to obtain $Q_{EC,}$ the mol[O_2].s^{-1} produced by the ionic current in the melt. This can be done by the linear extrapolation of the current-density values measured below 0.9 V, see

Figure 3, and their subsequent subtraction from the measured current-density above 0.9 V. An important requirement for this methodology is that current-density values used for the extrapolation are entirely of electronic nature. For further explanation please refer to [14]. The obtained Q_{EC} is then attributed to the ionic current. This ionic current corresponds in magnitude to the sum of anodic charge transfer that occurs via the oxidation of oxide anions, reaction (3), and of ferrous iron as per reaction (13).

Q_{ideal}, Q_m and Q_{EC} derived for the SLSV in the different compositions are shown in Figure 8 a-d in dependence of the cell voltage. For compositions Fe#5 and Fe#7.5 a superposition of Q_m and Q_{EC} can be seen between 1.1 V and 1.2 V. In this case, Q_{EC} is completely due the result of reaction (3), the oxidation of oxide anions. The fact that the

faradaic yield, shown in

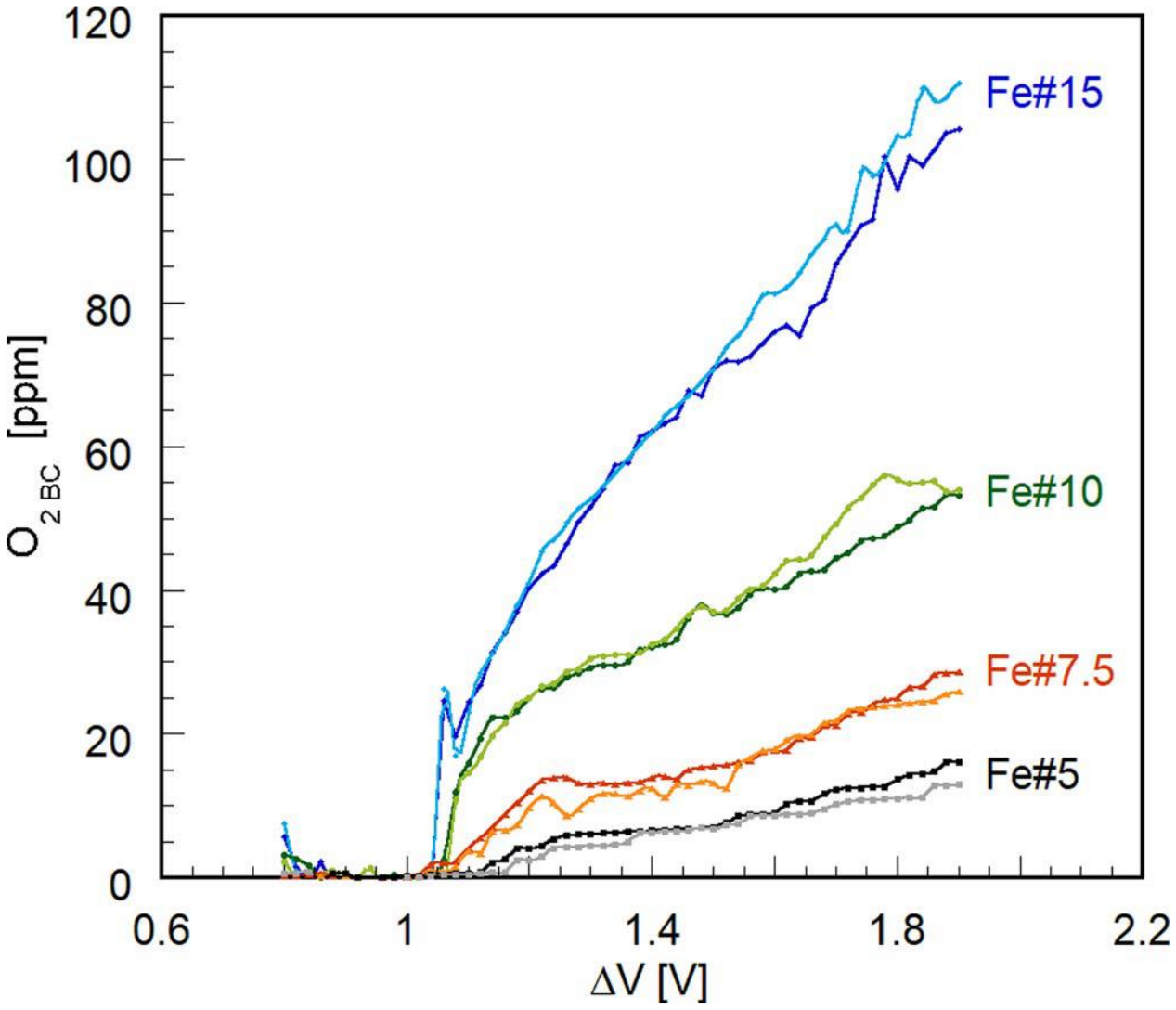

Figure **7**, is not exceeding 50 % for Fe#5 and Fe#7.5 suggests a proportionally high electronic contribution to the overall current in the silicate electrolyte. Above 1.2 V, Q_m remains stable while Q_{EC} continues to increase. The behavior of Q_m is observed in the plateau in O_2 production, see

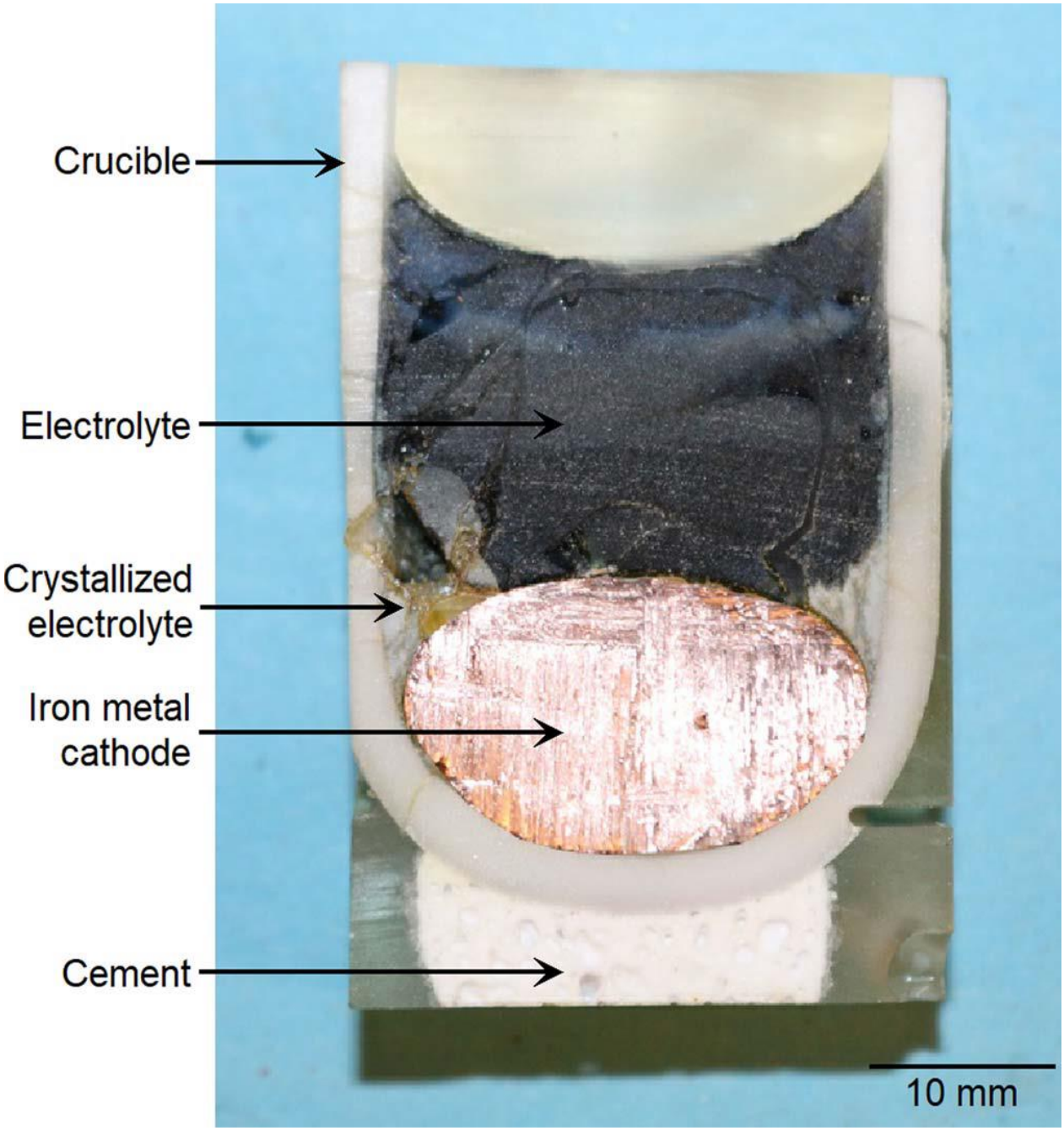

Figure **6**. As discussed above, it is most plausibly due to a mass transfer limitation of free oxide anions and leads to a decrease of the faradaic yield, see Figure 7. Once the faradaic yield decreases the derived Q_{EC} corresponds to the anodic charge transfer accomplished by the oxidation of oxide ions and ferrous iron, reaction (3) and (13) respectively.

Further increase of iron oxide leads to a change in the proportions of the different current partitions. In composition Fe#10 it is observed that Q_m is parallel to Q_{ideal} and in addition Q_m exceeds Q_{EC} in the cell voltage range from 1.1 to 1.3 V. This infers that the measured amount of O_2 gas exceeds the amount of O_2 derived from the ionic current. As this cannot be the case, it is presumed that the electronic current in Fe#10 is overestimated by using linear extrapolation of current values measured below 0.9 V. A reason for this might be that the current measured below 0.9 V is not solely electronic but a sum of electronic and of ionic conduction. An ionic current must be linked to an electrochemical reaction in the cell. Concerning their respective thermodynamic thresholds, reaction (6) and (7), the decomposition of FeO into Fe-metal and respectively Fe_3O_4 or Fe_2O_3, can take place below 1 V and thus allow the passage of an ionic current in the cell. At 1 V the thermodynamic threshold for the decomposition of FeO into Fe^0 and $O^{(II-)}$ via reaction (8) is exceeded and this reaction competes with reaction (6) and (7). The two latter reactions are linked to the oxidation of ferrous iron at the anode, reaction (13). The charge transfer at the anode will be performed by the electroactive species with the lowest kinetic limitation. In the voltage range 1-1.2 V, Q_m is almost equal to Q_{ideal} and thus only a small amount of charge transfer is achieved by the oxidation of ferrous iron at the anode, as per reaction (13). Conclusively, free oxide anions replace ferrous iron ions in the anode half reaction, most probably due to faster reaction kinetics. Due to this shift in the anode half reaction, the faradaic yield of the total current increases from 0 to 80%, as

displayed in

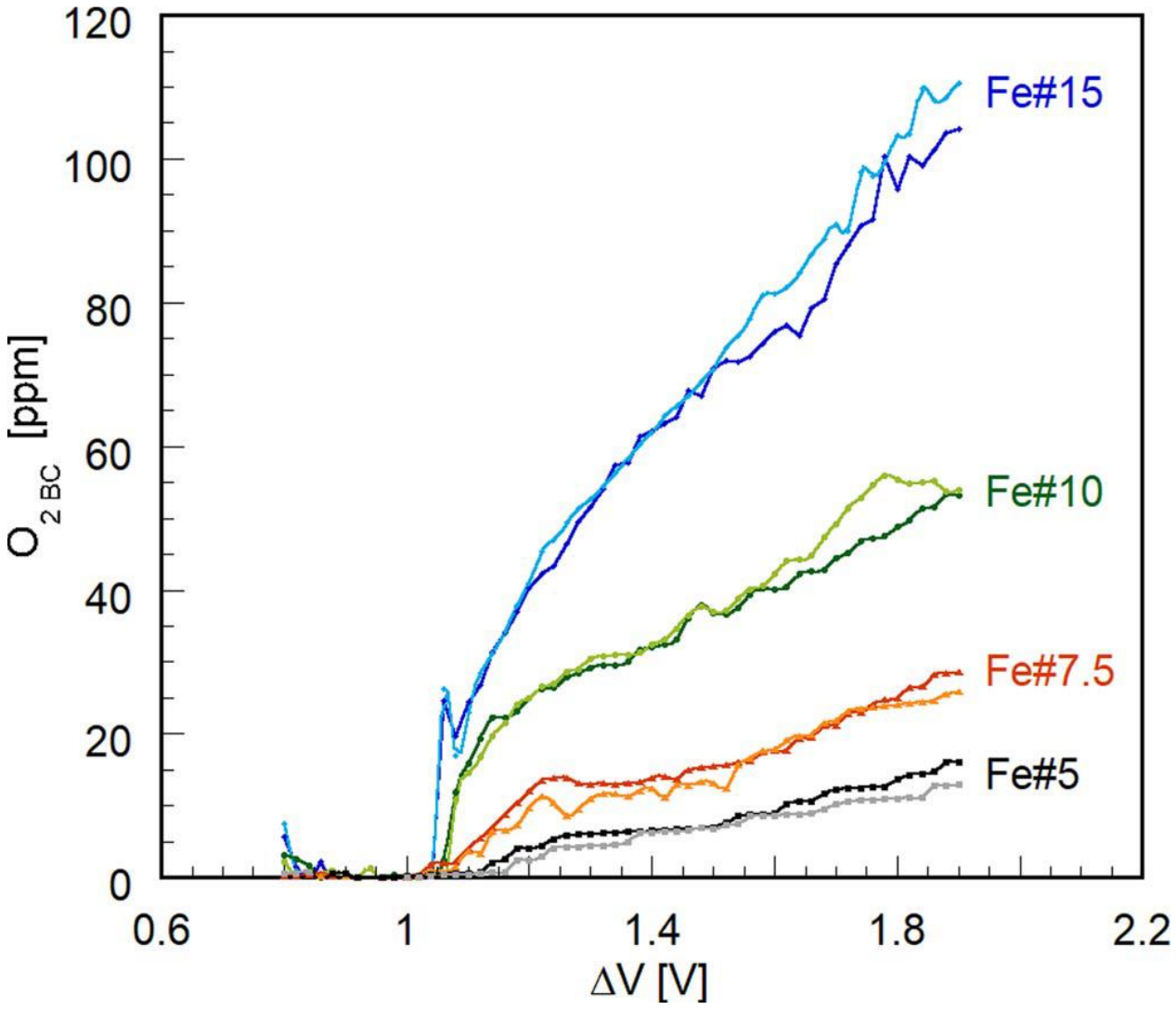

Figure **7**. The missing 20% are the sum of the electronic current in the cell and a remaining contribution of anodic ferrous iron oxidation via reaction (6) or (7). Similarly to Fe#5 and Fe#7.5, the electrochemical charge transfer at the anode would then occur in this cell voltage range almost entirely due to the oxidation of oxide anions. Above 1.2 V free oxide anions are no longer capable of serving a further increase of the cell voltage and ferrous iron ions participate significantly in the anode half reaction, leading to a significant decrease in the anode yield.

Increasing the iron oxide concentration to 15 wt% leads to a further increase of the current below 1 V. Extrapolation of these current values results in a Q_{EC} smaller than Q_m for the entire experiment. Despite the absence of O_2 gas evolution, it is concluded that the current below 1 V is partially ionic. The ionic current below 1 V is therefore linked to an oxidation of ferrous iron at the anode. The measured oxygen above 1 V in Fe#15 indicates that a large part of the charge transfer by the oxidation of ferrous iron is replaced by the oxidation of $O^{(II-)}$, once the thermodynamic threshold of reaction (8) is exceeded. This is in accordance with Fe#10. However, the constant anode yield of ~50 % obtained for

composition Fe#15, see

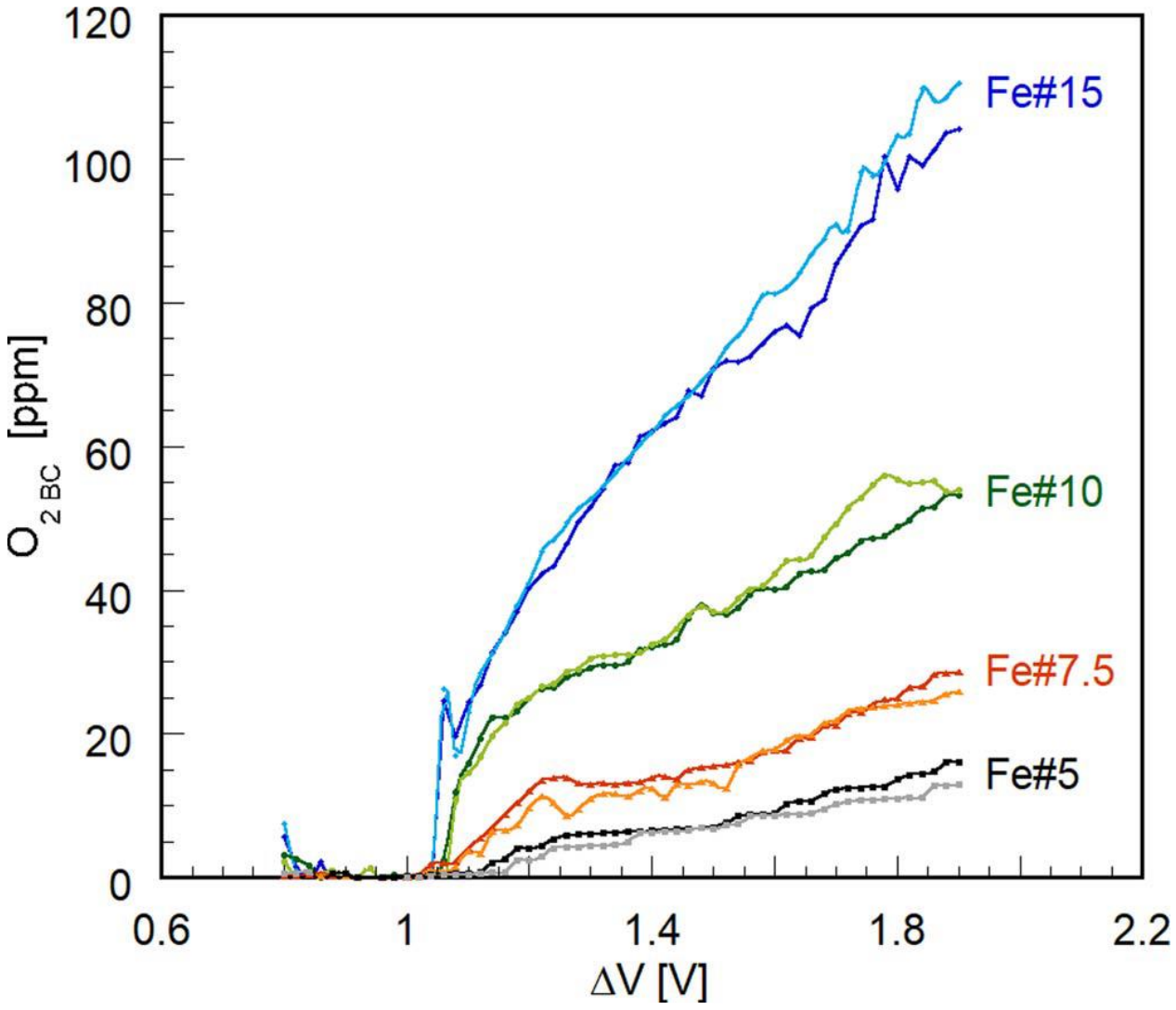

Figure **7**, suggests that the oxidation of $O^{(II-)}$ is not as electrochemically favored as for the other electrolytes. Ferrous iron participates continuously to a large part in the charge transfer at the anode. This behavior is the direct consequence of the high concentration of iron ions in the electrolyte. Since neither ferrous iron nor oxide anions seem to be limited by mass transfer at this iron oxide concentration, they contribute equally to the charge transfer. As a result, a mass transfer limitation is not observed for Fe#15 and the current increases almost linearly with cell voltage, see

Figure 3.

In summary it can be stated that the total faradaic yield for oxygen production in Fe#5 and Fe#7.5 is lower compared to Fe#10 and Fe#15 due to a proportionally higher electronic contribution of the silicate electrolyte to the current. Furthermore, it was shown that at low iron oxide concentrations free oxide anions are the electroactive species for the charge transfer at the anode. This result matches well with previous findings [7]. However, with increasing cell voltage ferrous iron additionally participates in the half cell reaction. At concentrations of more than 10 wt% FeO_x ferrous iron participates permanently in the anode half-reaction which is observed in the entire investigated range of cell voltages.

Proposition of a stepwise mechanism for the oxidation of oxide anions

The results presented in this study for oxygen gas production in dependence of the cell voltage highlight several key points. The first point is the development of O_2 due to the decomposition of iron oxides into iron metal and oxygen gas, reaction (8). Subsequently oxygen concentration in the argon gas flux increases with further augmentation of the cell voltage. However, in compositions Fe#5, Fe#7.5 and Fe#10 the measured levels of O_2 stabilize for a cell voltage range of up to 300 mV before increasing again for the remaining experiment, see Figure 4. As discussed above, this stabilization is most likely due to a mass transfer limitation of oxide anions. A mass transfer limitation would also apply to higher cell voltages and a subsequent increase of O_2 concentration, as observed in the results, should not occur. This behavior indicates a second process for the release of the O_2 gas. As the product of the anode half reaction remains the same, ΔE of the cell reaction is identical and thus the two steps of the O_2 production are not separated by a

thermodynamic threshold. If the two steps are described by different reaction kinetics, which might be due to a change of the electroactive species at the anode releasing the oxygen, the change in behavior of O_2 production should be sensitive to the current density. The relationship of oxygen production and current density is shown in

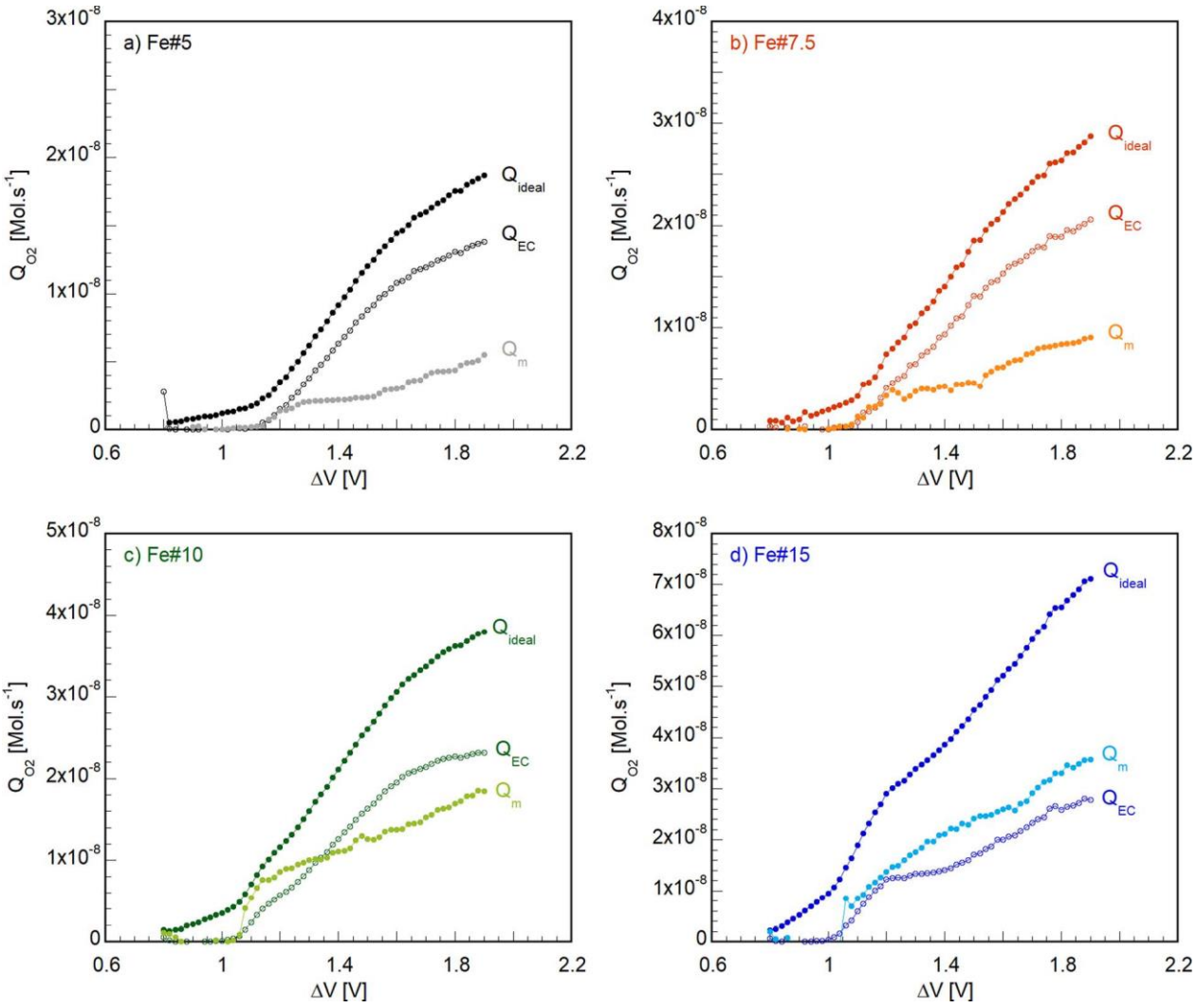

Figure **9**.

As for the voltammograms, a plateau is visible for compositions Fe#5 and Fe#7.5. Above the plateau the increase of O_2 production seems to follow a similar trend, which is indicated by the hachured line in the graph. The O_2 production registered in Fe#10 and Fe#15 aligns with this trend. Thus, above a certain current density in Fe#10 and Fe#15 charge transfer occurs in an analogue manner as in Fe#5 and Fe#7.5 above the supposed mass transfer limitations. If so, it can be assumed that once a respective critical current density is reached, the charge transferring mechanism is identical for any iron concentration in the investigated molten oxide system. The continuous change between the two mechanisms, as seen in Fe#10 and Fe#15, might explain why a clear diffusive current was not observed in previous studies [7].

For an explanation the different types of oxygen anions in the silicate network structure must be considered. Molten oxides contain multiple types of oxygen anions [22-24], namely free- ($O^{(II-)}$), non-bridging-(NBO) and bridging-oxygen anions (BO). NBO and BO come together with network forming cations (e.g. $Si^{(IV)}$) to create the structural network of the melt. Both are tightly bonded within the different structural units, such as $Si_2O_7^{(VI-)}$ or $Si_2O_6^{(IV-)}$, constituting the silicate network [25]. The charge transfer at the electrodes under anodic conditions is believed to be accomplished by free oxide anions [26-27] liberated from silica structural units following a polymerization reaction [28], such as that of reaction (15).

$$(\boldsymbol{Si_2O_6})^{(IV-)} \leftrightarrows (\boldsymbol{Si_2O_5})^{(II-)} + \boldsymbol{O}^{(II-)} \qquad (15)$$

Subsequently, the liberated oxide anion is oxidized at the electrode following equation (3). It has to be noted that the authors do not have exact knowledge of the present structural units in the electrolyte investigated here, thus reaction (15) is only given as an example.

Therefore, the mass transfer limitations in compositions Fe#5 and Fe#7.5 apply not only on the liberated oxygen but also on the abundancy of the structural unit polymerizing to provide the oxide anion. The second increase in O_2 levels might therefore be understood as a change in the polymerization reaction. If this second reaction is characterized by slower reaction kinetics, it might only take importance once reaction (15) and the oxidation of ferrous iron, reaction (13) are no longer able to support the applied potential. For MOE processing the results have a two-sided impact. On the one hand, a distinct limitation of the total current density is absent, which gives freedom to the anode design. On the other hand, only a small window exists for an operation at an anode yield close to unity based on the ionic current. For high concentrations of iron oxide, it seems difficult to restrict the charge transfer to oxide anions. Yet, ferric iron is unstable at operating conditions and it is possible that the formerly oxidized iron ions are thermally reduced after a certain time. This process is significantly slower than the electrochemical oxidation of ferrous iron and its impact on the process yield could only be shown in a continuous process. Indication of the relatively slow reaction rate of thermal reduction is given by the background measurement of oxygen, which proves the ongoing thermal decomposition of the introduced iron oxide following reaction (4).

Conclusion

The impact of multivalent metal cations on oxygen production through molten oxide electrolysis was investigated by means of a stepped linear scan voltammetry in an asymmetric electrode configuration at 1793 K. The results show that the overall yield for oxygen gas production increases with increasing electrolyte basicity as the electronic

contribution to the current becomes proportionally lower. However, the principal charge transferring anions at the anode are oxygen anions. With increasing iron oxide concentration, the influence of ferrous iron on the charge transfer is increased. Thus, the faradaic yield of the anode half reaction is negatively correlated to the electrolyte iron oxide content. Contrary to previous studies, multiple steps for the production of oxygen gas from the molten oxides have been observed. One plausible explanation for the stepwise increase might be a change of polymerization reaction liberating the oxygen anions. A coupling of the O_2 production and the current density leads to an assumption that this sequence is governed by the kinetics of the different polymerization reactions and of the oxidation of the ferrous iron in the melt.

References

[1] R. Winand, A. Fontana, L. Segers, L. Hannaert and J. Lacave, “Molten Salt Electrolysis in Metal Production”, Molten Salt Electrolysis Metal Production International Symposium, pp. 42-50, 1977.

[2] A. Allanore, “Features and Challenges of Molten Oxide Electrolytes for Metal Extraction”, J. Electrochem. Soc., vol. 162, pp. E13-E22, 2015.

[3] D. Wang, A. Gmitter and D. Sadoway, “Production of Oxygen Gas and Liquid Metal by Electrochemical Decomposition of Molten Iron Oxide”, J. Electrochem. Soc., vol. 158, n° 16, pp. E51-E54, 2011.

[4] H. Kim, J. Paramore, A. Allanore and D. R. Sadoway, “Electrolysis of Molten Iron Oxide with an Iridium Anode: the Electrolyte Basicity”, Journal of Electrochemical Society, vol. 158, pp. E101-E105, 2011..

[5] U. Pal, “A lower carbon footprint process for production of metals from their oxide sources”, Journal of Metals, vol. 2, pp. 43-47, 2008.

[6] J.-P. Birat, F. Hanrot and G. Danloy, “CO2 mitigation technologies in the steel industry: a benchmarking study based on process calculations”, Stahl und Eisen , vol. 123, n°19, pp. 69-72, 2003.

[7] A. H. Caldwell, E. Lai, A. J. Gmitter and A. Allanore, “Influence of Mass Transfer and Electrolyte Composition on Anodic Oxygen Evolution in Molten Oxides”, Electrochim. Acta, vol. 219, pp. 178-186, 2016.

[8] J. Stebbins, “Free oxide ions in silicate melts: Thermodynamic considerations and probable effects of temperature”, Chem. Geol., vol. 461, pp. 2-12, 2017.

[9] S. H. Lee and D. J. Min, “Influence of Basicity on Anodic Reaction in CaO-SiO_2-Al_2O_3 Melts”, J. Electrochem. Soc., vol. 164, n° 18, pp. H5308-H5314, 2017.

[10] J. Bockris, J. Kitchener and A. Davies, “Electric transport in liquid silicates”, Transactions of Faradaic Society, vol. 48, pp. 536-548, 1952.

[11] H. Inouye, J. W. Tomlinson and J. Chipman, “The Electrical Conductivity of Wüstite Melts”, Transactions of the Faraday Society, vol. 49, pp. 796-801, 1953.

[12] J. Wiencke, H. Lavelaine, P.-J. Panteix, C. Petitjean and C. Rapin, “Electrolysis of iron in a molten oxide electrolyte”, J. Appl. Electrochem., vol. 48, n° 11, pp. 115-126, 2018.

[13] K. A. Sasaki, Y. Hao and S. M. Haile, “Geometrically asymmetric electrodes for probing electrochemical reaction kinetics: a case study of hydrogen at the Pt–CsH_2PO_4 interface”, Phys. Chem. Chem. Phys., vol. 11, n° 137, pp. 8349-8357, 2009.

[14] J. Wiencke, H. Lavelaine, P.-J. Panteix, C. Petitjean and C. Rapin, “Kinetics of iron electrochemical reduction into liquid metal at 1823 K in a molten oxide electrolyte”, Mater. Chem. and Phys., vol. 212, pp. 214-223, 2018.

[15] J. Duffy and M. Ingram, “Establishment of an optical scale for Lewis basicity in inorganic oxyacids, molten salts and glasses”, J. Am. Chem. Soc., vol. 93, n° 124, pp. 6448-6454, 1971.

[16] B. Sundman, “An Assessment of the Fe-O System”, Journal of Phase Equilibria, vol. 12, n° 11, pp. 127-140, 1991.

[17] A. Ducret, D. Khetpal and D. R. Sadoway, “Electrical Conductivity and Transference Number Measurements of FeO-CaO-MgO-SiO_2 Melts”, Proc. Electrochem. Soc., pp. 347-353, 2002.

[18] R. Hundermark, “The Electrical Conductivity of Melter Type Slags”, Master's thesis, 2003.

[19] A. Bard, L. Faulkner, J. Leddy and C. Zoski, “Electrochemical methods: fundamentals and applications”, vol. 2, 1980.

[20] I. Barin, “Thermochemical Data of Pure Substances”, Wiley-VCH, 2004.

[21] C. Gatellier, H. Gaye, J. Lehmann and Y. Zbaczyniak, “Des outils Thermodynamiques pour la Maîtrise des Réactions Métal-Laitier and le Controlôle Inclusionnaire des Aciers”, Revue de Metallurgie, pp. 887-888, 1992.

[22] E. T. Turkdogan, “The Physicochemical Properties of Molten Slags and Glasses”, The Metals Society, 1983.

[23] K. C. Mills, “The Influence of Structure on the Physico-chemical Properties of Slags”, The Iron and Steel Institute of Japan International, vol. 33, pp. 148-155, 1993.

[24] B. Mysen and P. Richet, “Silicate glasses and melts”, Developments in Geochemistry, vol. 10, 2005.

[25] W. H. Zachariasen, “The atomic arrangement in glass”, J. Am. Chem. Soc., vol. 54, n° 110, pp. 3841-3854, 1932.

[26] A. Gosh and T. King, “Kinetics of Oxygen Evolution at a Platinum Anode in Lithium Silicate Melts”, Transactions of the Metallurgical Society of AIME, vol. 245, pp. 145-153, 1969.

[25] K. W. Semkov and L. A. Haskin, “Concentrations and behavior of oxygen and oxide ion in melts of composition $CaO \cdot MgO \cdot xSiO_2$”, Geochim. Cosmochim. Acta, vol. 49, n° 19, pp. 1897-1908, 1985.

[26] J.-Y. Tilquin, J. Glibert and P. Claes, “Anodic Polarization of Silicates”, J. Non-Cryst. Solids, vol. 188, pp. 266-274, 1995.

List of Tables

Table 1: List of chemical substances used for the electrolyte

	Supplier	Grainsize	Purity [%]
SiO_2	Alfa Aesar	≤ 10 µm	99.5
Al_2O_3	Alfa Aesar	≤ 1 mm	98
MgO	Alfa Aesar	≤ 100 nm	99+
Fe_3O_4	Aldrich	≤ 5 µm	98

Table 2: Compositions of starting material and molten oxide electrolytes together with their respective optical basicity (Λ)

	SiO_2 [wt%]	Al_2O_3 [wt%]	MgO [wt%]	Fe_3O_4 [wt%]	Λ
Fe#0	66.0	20.0	14.0	0.0	0.519
Fe#5	62.7	19.0	13.3	5.0	0.531
Fe#7.5	61.0	18.5	13.0	7.5	0.537
Fe#10	59.4	18.0	12.6	10.0	0.544
Fe#15	56.1	17.0	11.9	15.0	0.557

Table 3: Possible reactions in the investigated voltage interval for the different compositions

	Thermodynamic reaction	Reaction potential [V]			
		Fe#5	Fe#7.5	Fe#10	Fe#15
(6)	$4FeO \leftrightarrows Fe^0 + Fe_3O_4$	0.69	0.67	0.65	0.63
(7)	$3FeO \leftrightarrows Fe^0 + Fe_2O_3$	0.86	0.83	0.81	0.79
(8)	$2FeO \leftrightarrows 2Fe^0 + O_2$	1.04	1.02	1.00	0.98
(9)	$SiO_2 \leftrightarrows Si^0 + O_2$	1.51	1.51	1.51	1.51
(10)	$2SiO_2 \leftrightarrows 2SiO + O_2$	1.72	1.72	1.72	1.72
(11)	$2Al_2O_3 \leftrightarrows 4Al^0 + 3O_2$	1.93	1.93	1.93	1.93
(12)	$2MgO \leftrightarrows 2Mg^0 + O_2$	1.96	1.96	1.96	1.96

Figure 1: Experimental set-up with large surface cathode

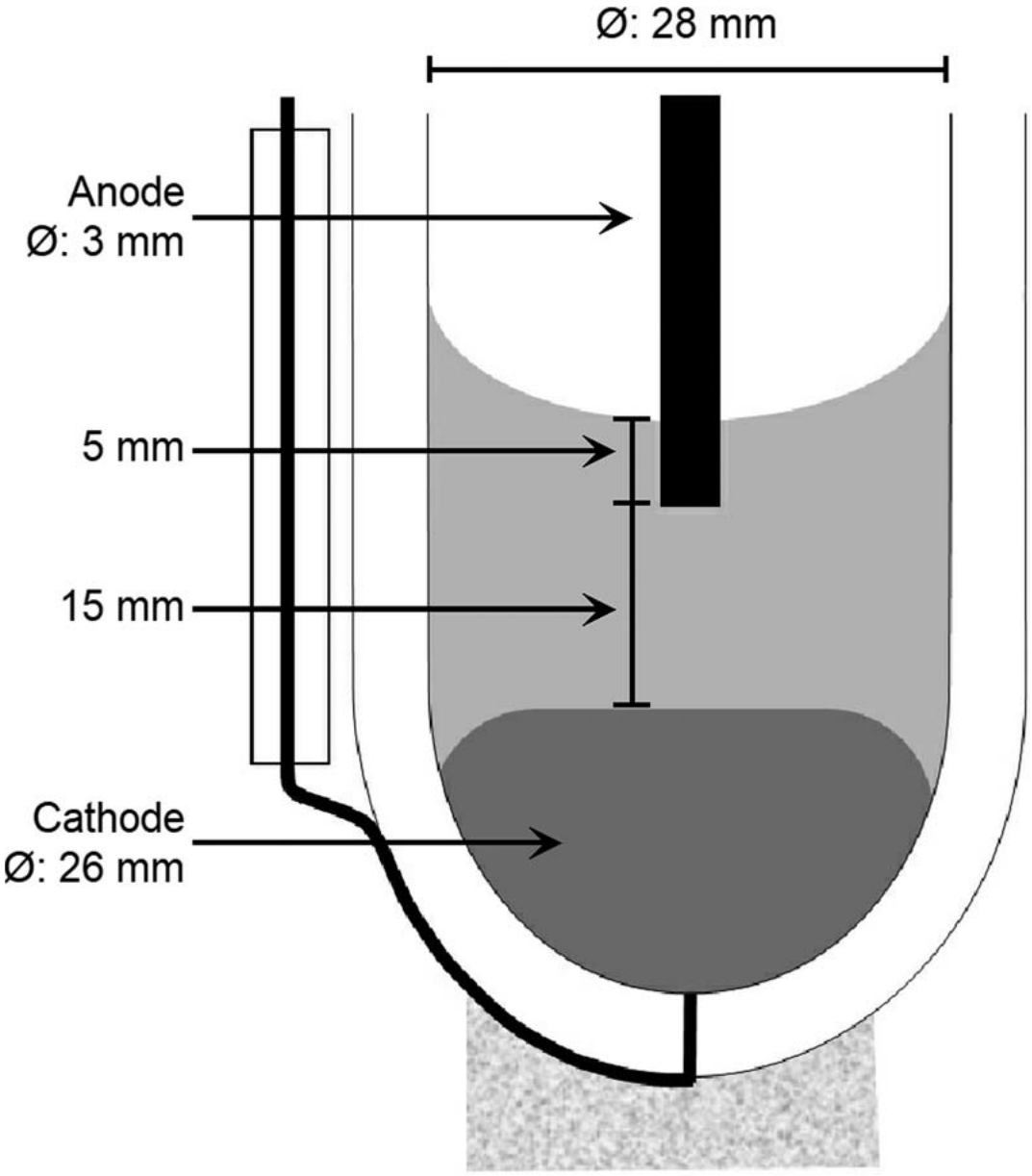

Figure 2: The electric field in the large surface cathode experimental set-up

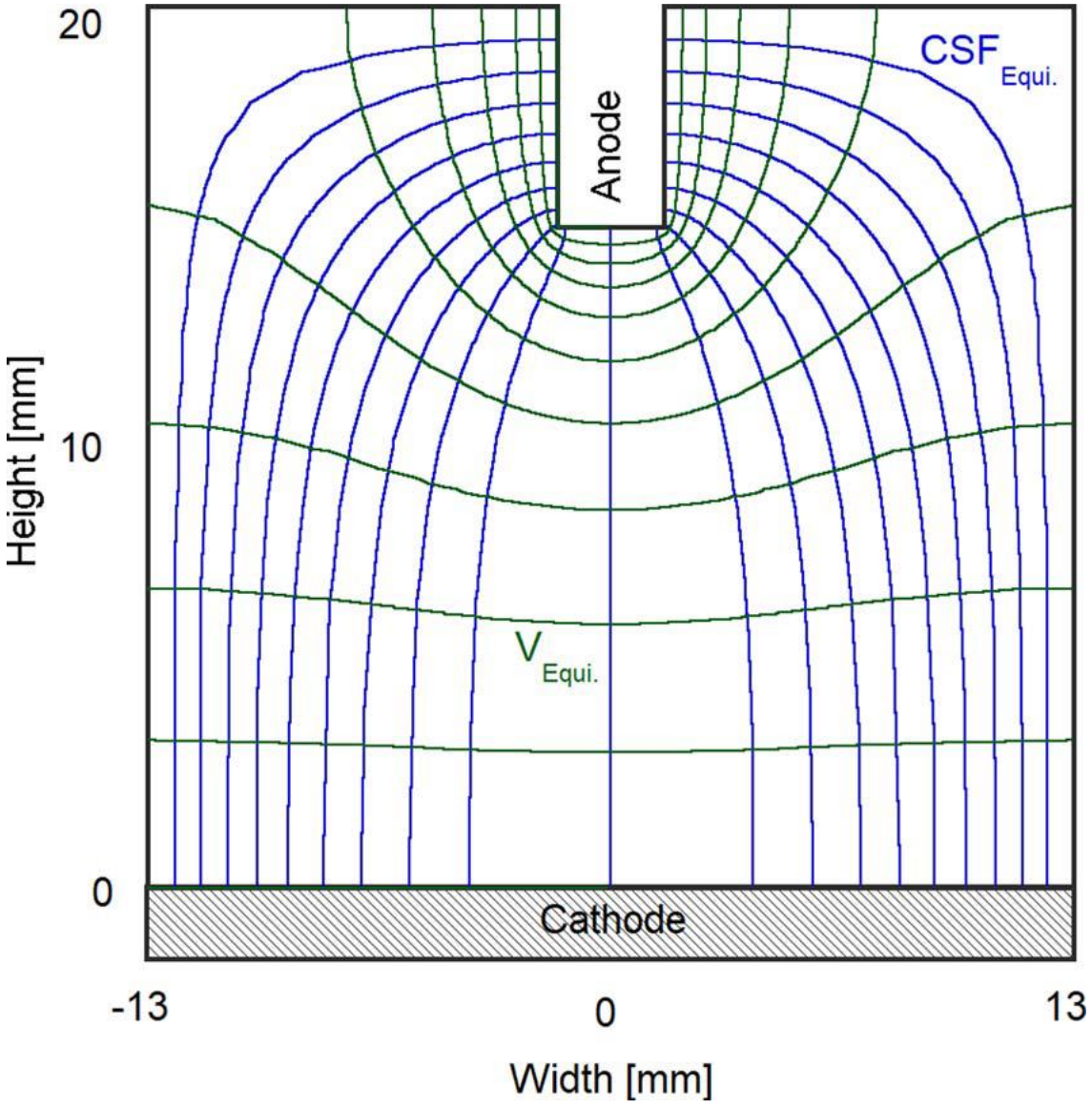

Figure 3: Measured current density in dependence of the applied cell voltage
Temperature: 1793 K±3, Ar-gas flow: 0.05 STP $m^3.h^{-1}$, Scanning rate 0.03 $mV.s^{-1}$

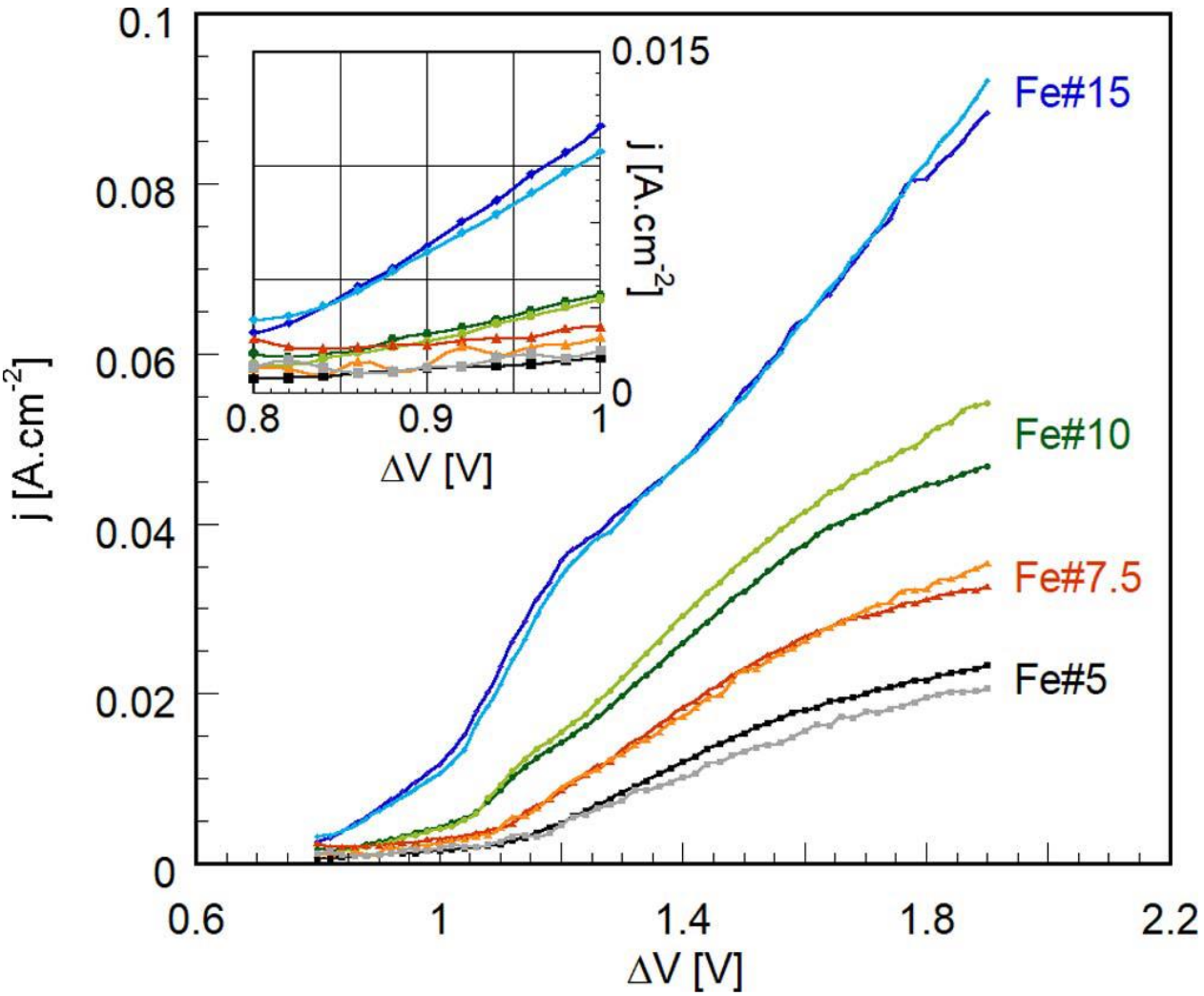

Figure 4: Measured oxygen concentration in Argon flow versus the applied cell voltage
Temperature: 1793 K±3, Ar-gas flow: 0.05 STP $m^3.h^{-1}$, Scanning rate 0.03 $mV.s^{-1}$

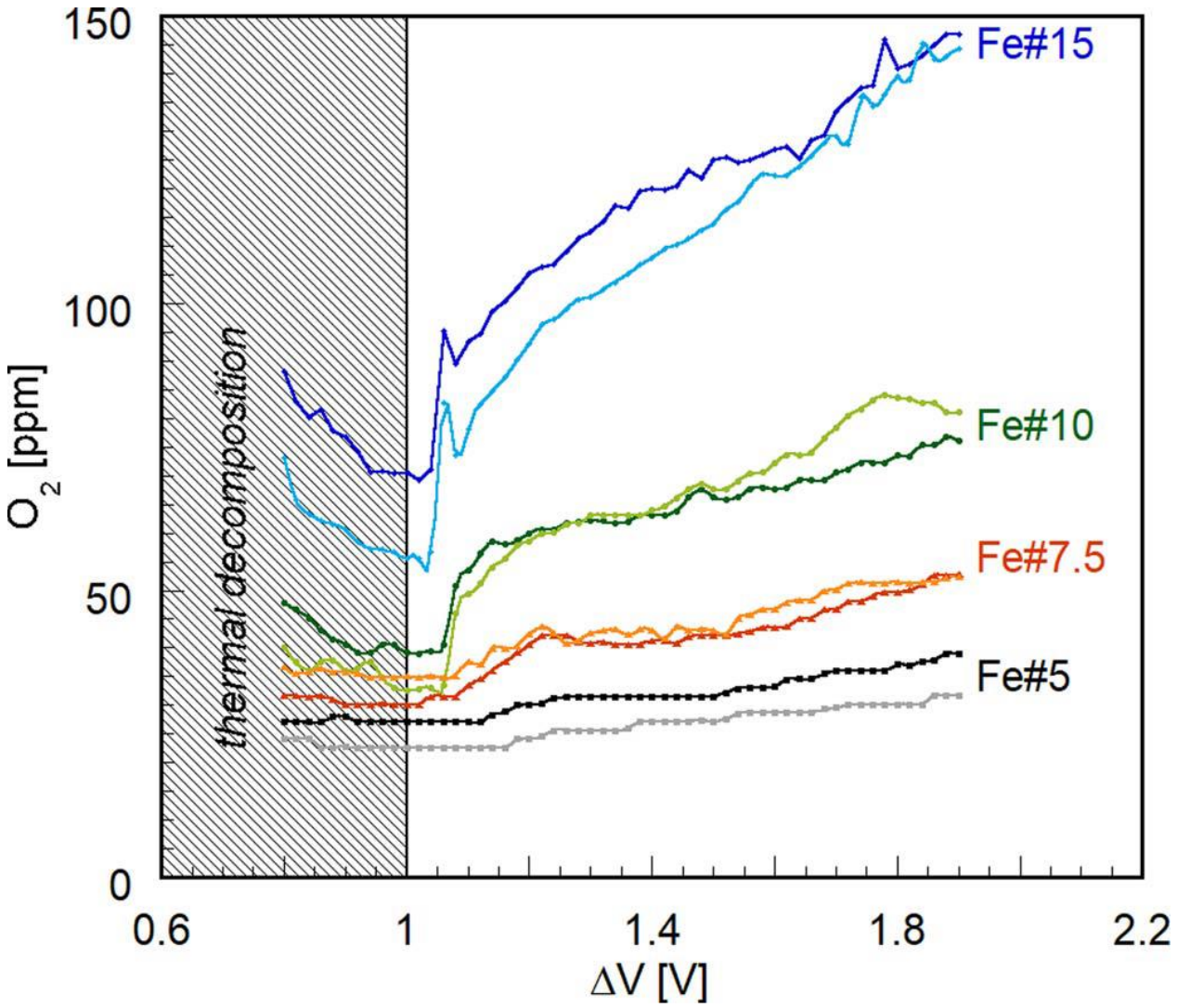

Figure 5 Electrochemical cell after the experiment with electrolyte Fe#15

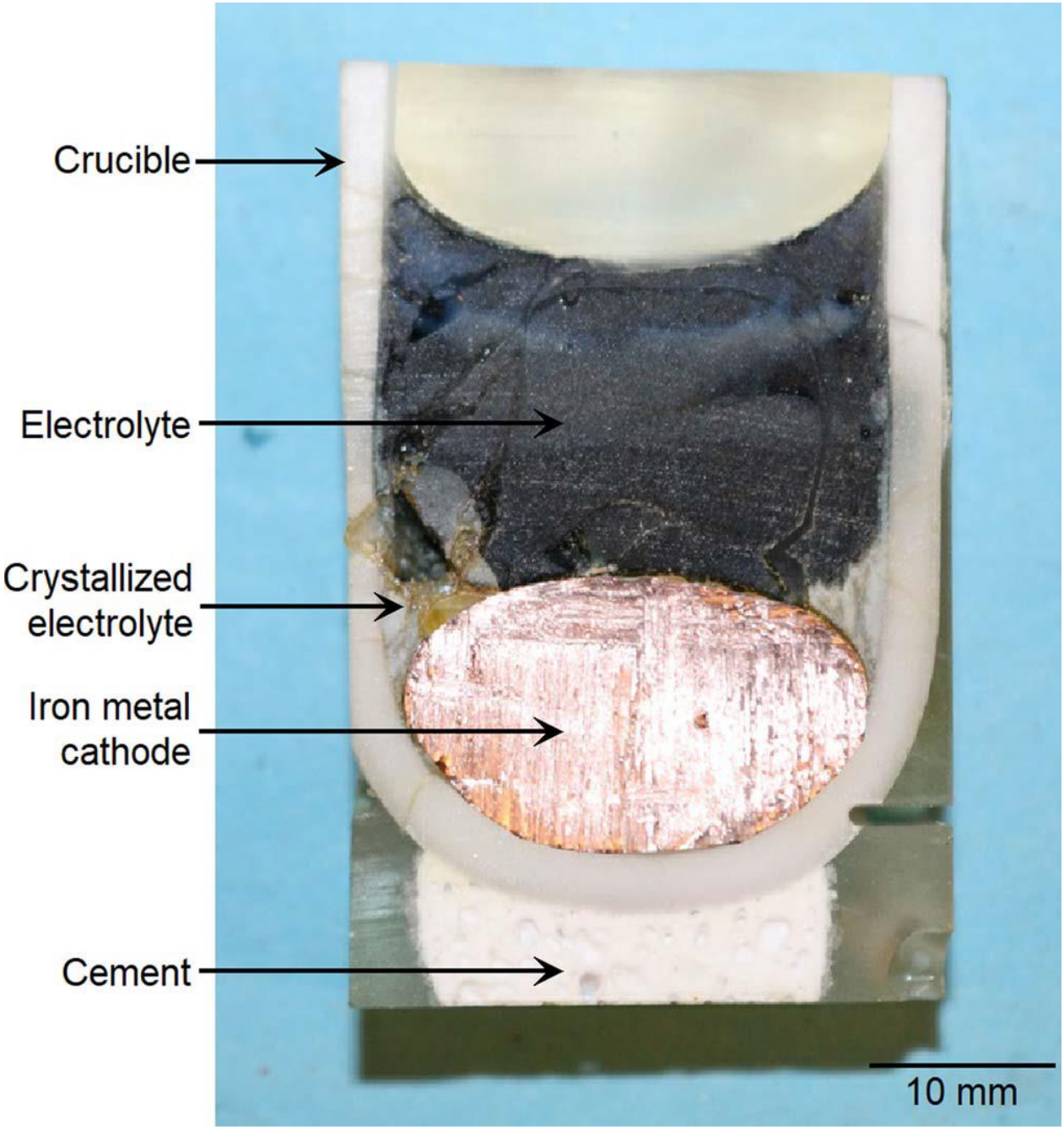

Figure 6: Background corrected oxygen concentration in Argon flow, $O_{2\,BC}$, in dependence of the applied cell voltage
Temperature: 1793 K±3, Ar-gas flow: 0.05 STP $m^3.h^{-1}$, Scanning rate 0.03 $mV.s^{-1}$

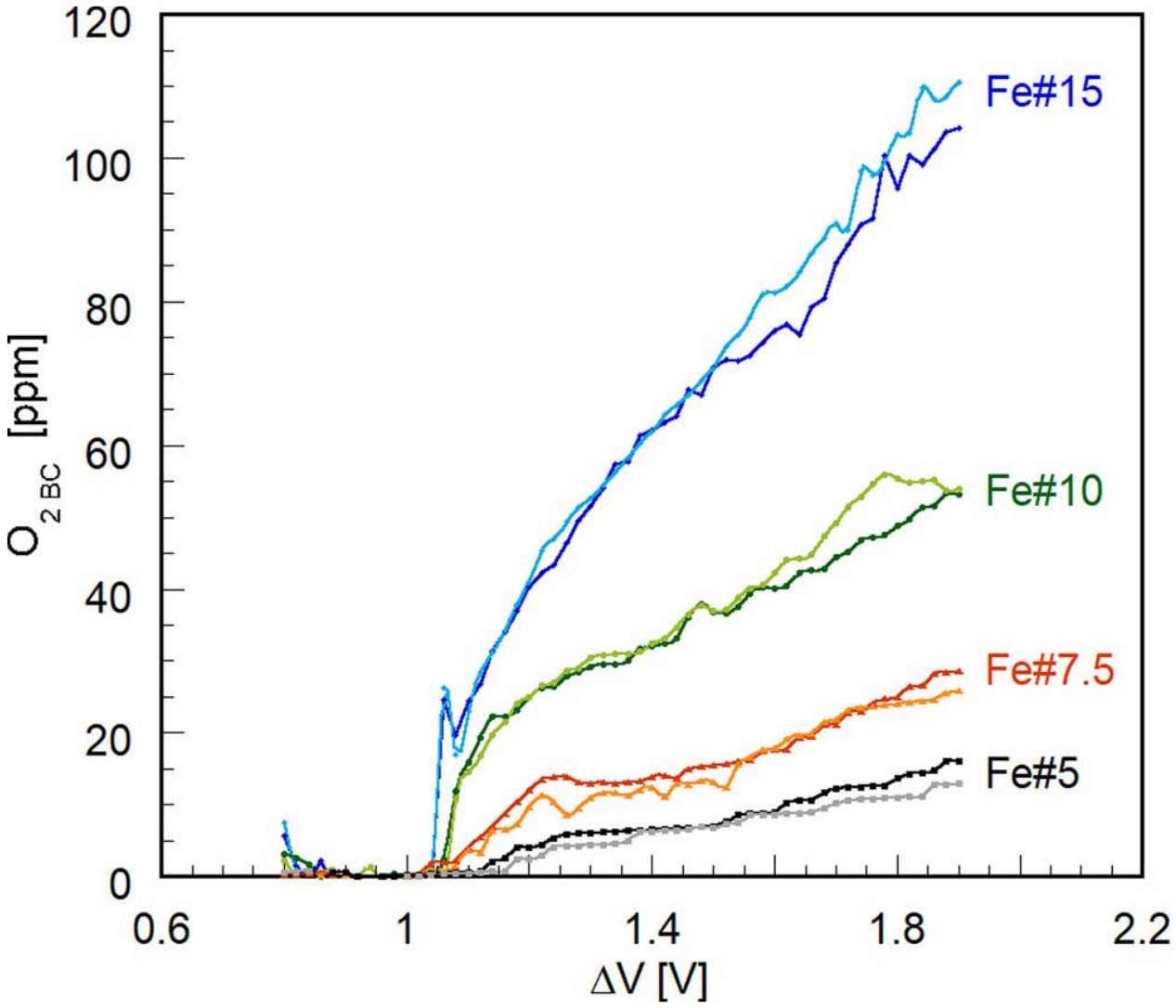

Figure 7: Faradaic yield identified for the different electrolyte compositions
Temperature: 1793 K±3, Ar-gas flow: 0.05 STP $m^3.h^{-1}$, Scanning rate 0.03 $mV.s^{-1}$

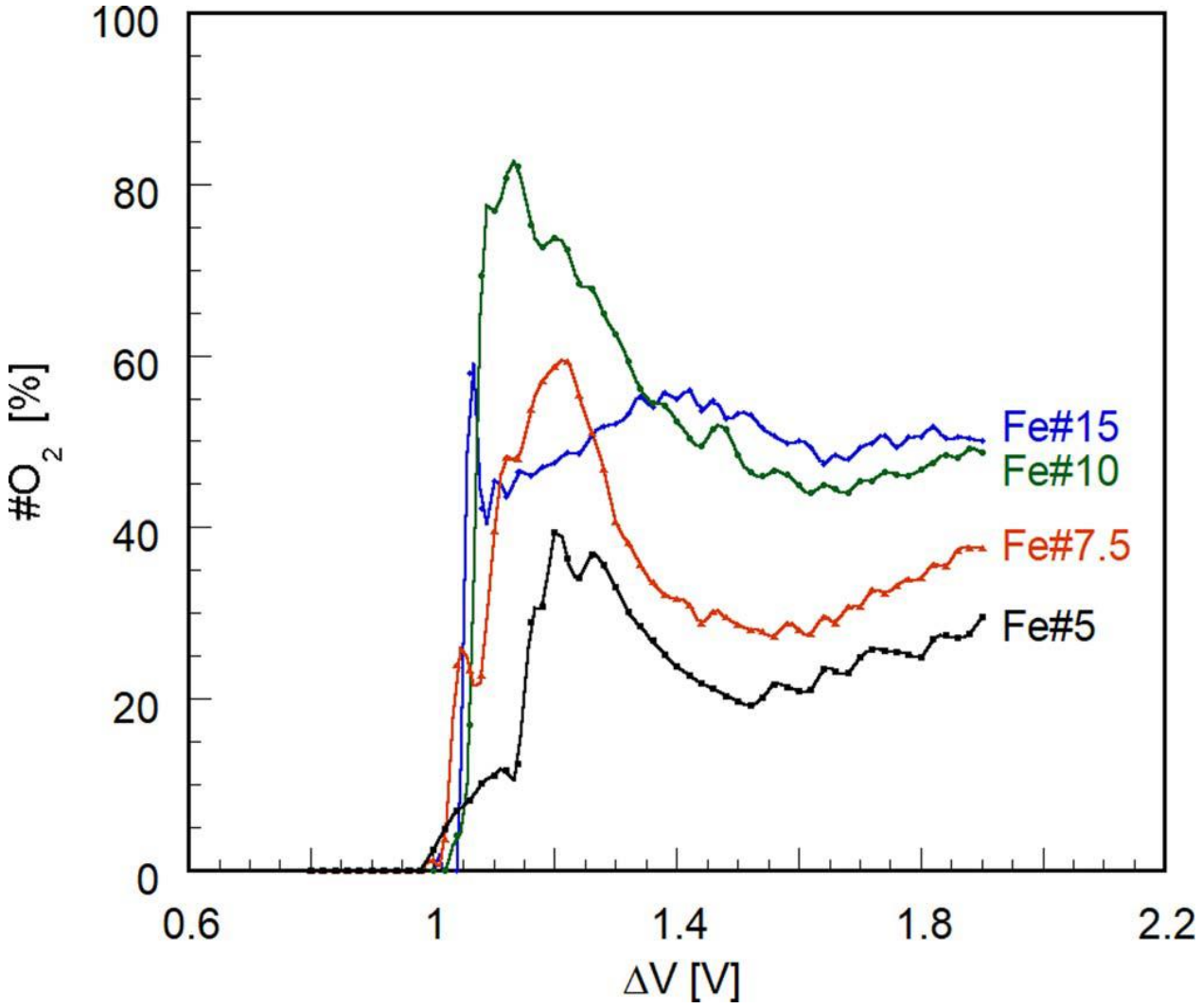

Figure 8: Comparison between the measured debit of O_2 (Q_m) and theoretical debits of O_2 derived for the measured current (Q_{ideal}) and for the ionic charge transfer (Q_{EC}) Temperature: 1793 K±3, Ar-gas flow: 0.05 STP $m^3.h^{-1}$, Scanning rate 0.03 $mV.s^{-1}$

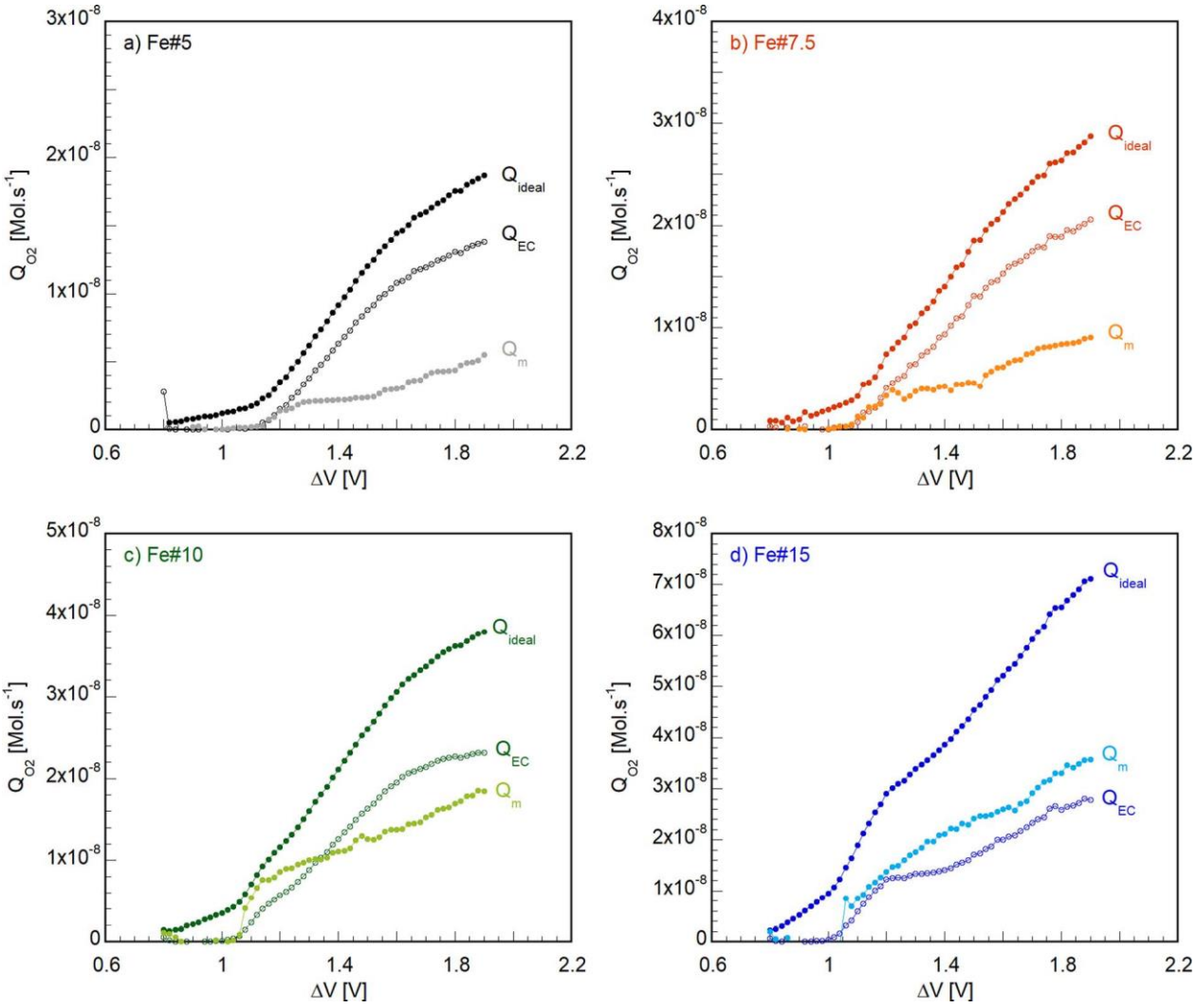

Figure 9: Background corrected O_2 level in dependence of the anode current density
Temperature: 1793 K±3, Ar-gas flow: 0.05 STP $m^3.h^{-1}$, Scanning rate 0.03 $mV.s^{-1}$